


Post your
ad today 

nature
careers



Geotechnical and Geological Engineering

An International Journal

[Geotechnical and Geological Engineering](#) > [Volumes and issues](#) > [Volume 40, issue 9](#)

Search within journal

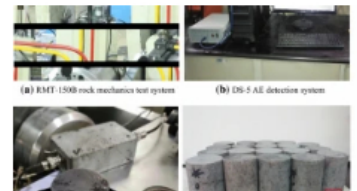

Volume 40, issue 9, September 2022

32 articles in this issue

[Effect of Strain Rate on Mechanical Properties and AE Characteristics of Hard Rock Under the Impact of Uniaxial Compression](#)

Pengfei Liu, Junqi Fan ... Fuli Kong

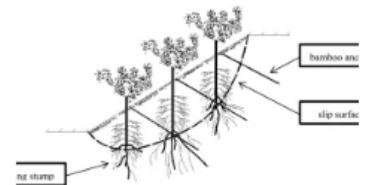
Original Paper | Published: 03 August 2022 | Pages: 4313 - 4326



[Model Test Studies on Slope Supported by Bamboo Anchor and Timber Frame Beam](#)

Xueliang Jiang, Yonghui Qian ... Jiahui Guo

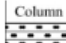





Original Paper | Published: 23 May 2022 | Pages: 4327 - 4344



[Influencing Factors of the Rebreak of the Key Rock Block of the Main Roof in the Gob](#)

Yang Li, Yuqi Ren ... Xinghai Lei

Original Paper | Published: 25 May 2022 | Pages: 4345 - 4356

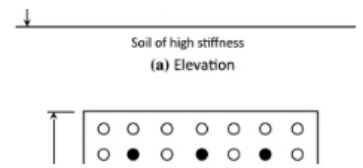
Column	Name	Average thickness	Lithology
	Main roof	7.30m	Siltstone
	immediate roof	2.60m	Carbonaceous mudstone
	False roof	0.60m	Carbonaceous mudstone
	Coal seam	3.40m	No.12 ₁ coal seam
	Immediate floor	6.25m	Siltstone
	Main floor	4.65m	Pine sandstone

A Simplified Method for the Nonlinear Analysis of Composite Piled Raft

[Foundation](#)

Basuony M. El-Garhy

Original Paper | Published: 18 May 2022 | Pages: 4357 - 4375

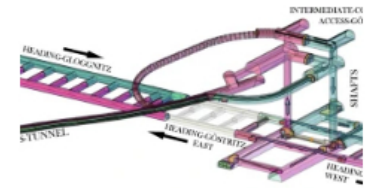


[Drilling and Grouting Works for Pressurised Groundwater Conditions of the Semmering Base Tunnel](#)

Helmut Wannenmacher, Manuel Entfellner & Hannes Hauer

Original Paper | [Open Access](#) | Published: 08 June 2022 | Pages: 4377 - 4391

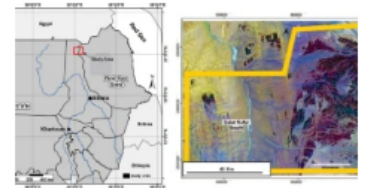
[This is part of 1 collection](#)



[Assessment of Rock Slope Instability of the Proposed Galat Sufar Open Pit Mine, River Nile State, Sudan](#)

Mohaned A. H. Bashir & Esamaldeen Ali

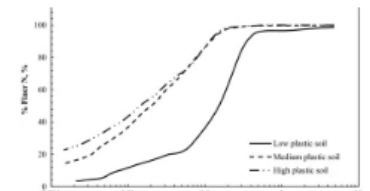
Original Paper | Published: 04 June 2022 | Pages: 4393 - 4418



[Natural Rubber Latex for Improving Ductility Characteristics of Soil: A Preliminary Experimental Investigation](#)

U Veena & Naveen James

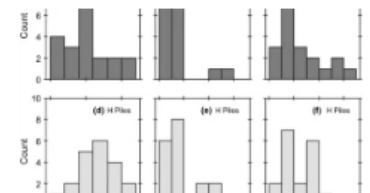
Original Paper | Published: 26 May 2022 | Pages: 4419 - 4446



[Reliability-Based Serviceability Limit State Design of Driven Piles in Glacial Deposits](#)

Markus Jesswein & Jinyuan Liu

Original Paper | Published: 03 June 2022 | Pages: 4447 - 4471



[Implementing Digital Imaging for Improved Understanding of Microfine Cement Grout Permeation and Filtration](#)

Chadi El Mohtar, Hamza Jaffal ... Katie Ward

Original Paper | Published: 28 May 2022 | Pages: 4473 - 4485

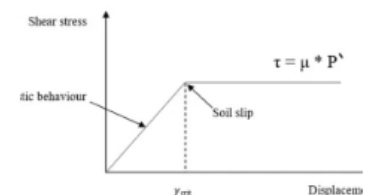
[This is part of 1 collection](#)



[Improved Pile Geometry to Reduce Negative Skin Friction on Single Driven Pile and Pile Groups Subjected to Lateral Loads](#)

Omar shawky, Ayman I. Altahrany & Mahmoud Elmeligy

Original Paper | Published: 07 June 2022 | Pages: 4487 - 4516



[Study of Deep In-Situ Stress Field Based on Geological Structures](#)

Jianguo Zhang & Peitao Li

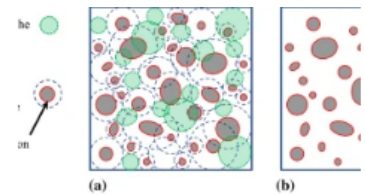
Original Paper | Published: 20 May 2022 | Pages: 4517 - 4527



[Effect of Particles Shape on the Hydraulic Conductivity of Stokesian Flow in Granular Materials](#)

Mehdi Veiskarami, Leila Roshanali & Ghassem Habibagahi

Original Paper | Published: 14 June 2022 | Pages: 4645 - 4656



[Deformation Characteristics and Mechanism of Side Walls of Wudongde Hydropower Station](#)

Lu Weiyong & He Changchun

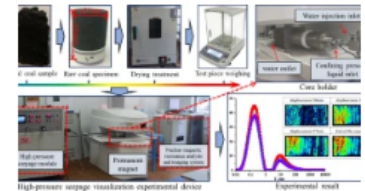
Original Paper | Published: 30 May 2022 | Pages: 4657 - 4671



[Fractal Characterization of Fracture Structure of Coal Seam Water Injection Based on NMR Experiment](#)

Zhen Liu, Wenzhi Yang ... Peng Hu

Original Paper | Published: 24 May 2022 | Pages: 4673 - 4684



[Developing the Rule of Thumb for Evaluating Penetration Rate of TBM, Using Binary Classification](#)

Mohammadreza Akbarzadeh, Sina Shaffiee Haghshenas ... Reza Mikaeil

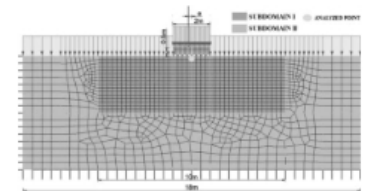
Original Paper | Published: 30 May 2022 | Pages: 4685 - 4703



[Effectiveness of Random Field Approach in Serviceability Limit State Analysis of Strip Foundation](#)

Karol Winkelmann, Kamil Żyliński ... Jarosław Górski

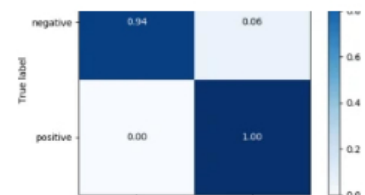
Original Paper | [Open Access](#) | Published: 06 June 2022 | Pages: 4705 - 4720



[A Comparative Study of Soil Liquefaction Assessment Using Machine Learning Models](#)

Shadi M. Hanandeh, Wassel A. Al-Bodour & Mustafa M. Hajj

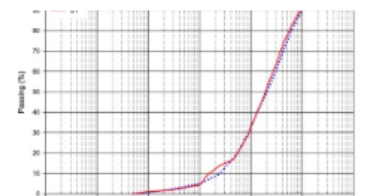
Original Paper | Published: 17 June 2022 | Pages: 4721 - 4734



[Behaviour of Backfill Undergoing Cementation Under Cyclic Loading](#)

Imad Alainachi, Mamadou Fall & Muslim Majeed

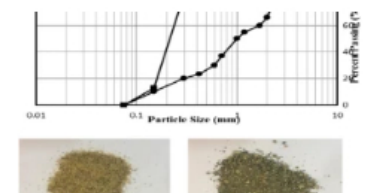
Original Paper | Published: 09 June 2022 | Pages: 4735 - 4759



[Appraisal of Anchor Arrangement and Size on Sand-Geogrid Interaction in Direct Shear](#)

Mahmood Reza Abdi & Mehdi Pour-Ramazan Chafjiri

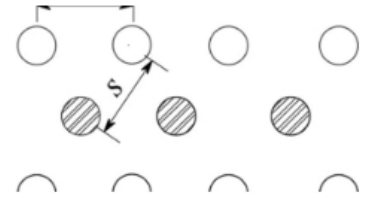
Original Paper | Published: 04 June 2022 | Pages: 4761 - 4773



[Performance of High Speed Railway Subgrade Strengthened by Long-Short Piles —Part I: Experimental Results](#)

Xuansheng Cheng, Lingyu Xia ... Yingchao Zhou

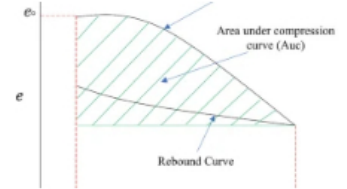
Original Paper | Published: 13 June 2022 | Pages: 4775 - 4785



[Development of a Compressibility Prediction Model Based on Soil Index Properties and Area Under/Bounded by Consolidation and Rebound Curves](#)

Muwafaq Awad, Abdulrahman Aldaood & Ibrahim Alkiki

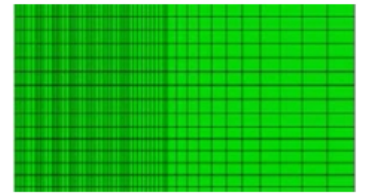
Original Paper | Published: 04 June 2022 | Pages: 4787 - 4807



[Performance of High Speed Railway Subgrade Strengthened by Long-Short Piles: Part II—Numerical Modelling](#)

Xuansheng Cheng, Lingyu Xia ... Yingchao Zhou

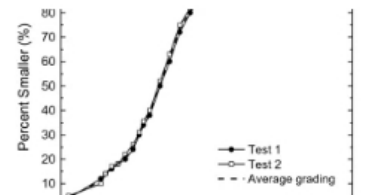
Original Paper | Published: 14 June 2022 | Pages: 4809 - 4820



[Predicting the Isotropic Volumetric Compression Response of Hydrating Cemented Paste Backfill \(CPB\)](#)

Mohammadamin Jafari & Murray Grabinsky

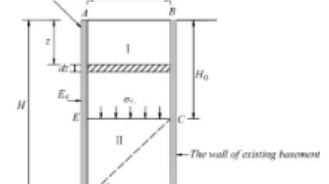
Original Paper | Published: 13 June 2022 | Pages: 4821 - 4836



[Estimation of Active Earth Pressure for Limited Width of Soil Using Nonlinear Failure Criterion](#)

Lu Cong, Xuan-yu Yang ... Wei Xiong

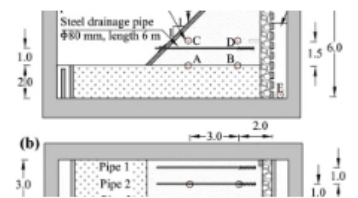
Original Paper | Published: 26 May 2022 | Pages: 4837 - 4846



[Comparative Performance of Steel Drainage Pipes Against Flood-Induced Deformation in River Levee](#)

Jenisha Singh, Kazuki Horikoshi ... Akihiro Takahashi

Technical Note | Published: 31 May 2022 | Pages: 4847 - 4857



For authors


[Submission guidelines](#)

[Manuscript editing services](#)

[Ethics & disclosures](#)

[Open Access fees and funding](#)

[Contact the journal](#)

Submit manuscript 



Working on a manuscript?

Avoid the most common mistakes and prepare your manuscript for journal editors.

[Learn more](#) →

Explore

[Online first articles](#)

[Volumes and issues](#)

[Collections](#)

Sign up for alerts

Advertisement

nature
masterclasses

**Boost your skills
with training
developed for
researchers**

Find out more



Over 10 million scientific documents at your fingertips

[Academic Edition](#) | [Corporate Edition](#)

[Home](#) | [Impressum](#) | [Legal information](#) | [Privacy statement](#) | [California Privacy Statement](#) | [How we use cookies](#) | [Manage cookies/Do not sell my data](#) | [Accessibility](#) | [FAQ](#) | [Contact us](#) | [Affiliate program](#)

Not logged in - 103.165.127.11

Not affiliated

SPRINGER NATURE

© 2023 Springer Nature Switzerland AG. Part of [Springer Nature](#).



Role of Actual Evaporation on the Stability of Residual Soil Slope

Nurly Gofar · Alfredo Satyanaga ·
Robby Yussac Tallar · Harianto Rahardjo

Received: 14 January 2022 / Accepted: 2 May 2022
© The Author(s), under exclusive licence to Springer Nature Switzerland AG 2022

Abstract Tropical countries like Singapore are associated with high relative humidity, high temperature, and high amount of rainfall throughout the year. Therefore, flux boundary conditions of slopes are affected by rainwater infiltration and evaporation rate. The research aims to examine the stability of a residual soil slope under arid and damp period conditions. The actual evaporation was utilized in combination with rainfall as flux boundary conditions in the mathematical investigations to study the impact of actual evaporation on the distribution of pore-water pressure and factor of safety variation in residual soil slope. The significance level of actual evaporation in the stability analysis of residual soil slope was tested by performing two instances of seepage analysis on a

slope subjected to (1) rainfall only and (2) rainfall and estimated evaporation. The data from the field instrumentation was compared with pore-water pressure variations in residual soil. It was observed that actual evaporation should be incorporated in the numerical analyses as a flux boundary condition in addition to rainfall loading since both actual evaporation and rainfall have a significant effect in generating accurate factor of safety variations and pore-water pressure distribution within soil layers.

Keywords Unsaturated soil · Landslides · Finite-element modelling · Seepage

N. Gofar
Postgraduate Program Universitas Bina Darma,
Palembang, Indonesia

A. Satyanaga (✉)
Department of Civil and Environmental Engineering,
School of Engineering and Digital Sciences, Nazarbayev
University, Nur-Sultan 010000, Kazakhstan
e-mail: alfredo.satyanaga@nu.edu.kz

R. Y. Tallar
Department of Civil Engineering, Universitas Kristen
Maranatha (Maranatha Christian University), Bandung,
Indonesia

H. Rahardjo
School of Civil and Environmental Engineering, Nanyang
Technological University, Singapore, Singapore

1 Introduction

The boundary interchange of water between the ground and atmospheric air usually takes place due to two procedures: rainfall evaporation and infiltration (Pierre et al. 2019; Rahardjo et al. 2014). Shifts in the boundary conditions of flux produce a flow with unsteady-state unsaturated/saturated parameters, which lead to an adjustment in the shear strength of the soil and pore-water pressure, and subsequently, stability of slopes (Fredlund and Rahardjo 1993; Ip et al. 2021; Satyanaga and Rahardjo 2020). To avoid greater unpredictability in their analyses of pore-water pressure and slope stability, many researchers consider only rainfall as the flux boundary condition (Ng et al. 2008; Li et al. 2005; Fredlund et al. 2012).

However, other researchers included the effect of evaporation and rainfall infiltration on the forecast of pore-water pressure variation in soil slopes (Gitirana et al. 2006; Raj et al. 2017).

Evaporation in the natural environment is one of the main phases of the hydrological cycle. Evaporation rate can be measured directly or predicted based on climate data. In the past few decades, many researchers have studied the mechanism of evaporative flow in different ways. The relationship between evaporation, solar radiation and other heat flux components in an energy budget context was also implicit in the previous works by accepting the energy budget concept. Three major factors that affect surface evaporation (Newson and Fahey 2003) are the availability of water within the evaporation surface, the energy of the evaporation and the aerodynamic function. The availability of water is a function of the water permeability and the water content of the soil (Newson and Fahey 2003; Zhai et al. 2019a, b). To date, many

climatological methods have been used to predict the potential evaporation. Those theories commonly only require typical climatic data: i.e., relative humidity, temperature and net radiation. These theories were established based on saturated soil surface or free water surface with certain limitations in applying it to the unsaturated soil surface. However, they still can be used as a reference to estimate the evaporation of the soil surface, that is considered suitable for many geotechnical applications (Table 1).

The objective of this research paper is to investigate the influence of rainwater infiltration and evaporation on pore-water pressure and factor of safety distributions for the residual soil slopes in Singapore. Seepage analyses were conducted on an instrumented slope at Orchard Boulevard Singapore utilizing flux boundary conditions from rainfall only and a combination of rainfall and actual evaporation calculated using Tran et al. (2015). Pore-water pressure information that was gathered from the instrumented slope

Table 1 Different theories to calculate potential evaporation

Equation	Theory	Definition of parameters	Equation No
$PE = 0.44(1 + 0.118u)(p_v - p_v^a)$	Mass transfer Rohwer (1931)	u = wind speed (miles/hour); p_v^a = vapour pressure above surface unaffected by evaporation; p_v = vapour pressure at the surface;	1
$PE_{(x_o, y_o)} = Cu_2^{0.76} x_0^{0.88} y_o (p_v - p_v^a)$	Thornthwaite and Holzman (1942)	x_o, y_o = evaporating area (m); C = constant related to temperature; u_2 = wind speed at 2 m (miles/day)	2
$PE = 1.6 \left(\frac{L}{12} \right) \left(\frac{N}{30} \right) \left(\frac{10T_a}{30} \right)^a$	Thornthwaite (1948)	N = frequency of days every month; L = duration of daylight (hours); T_a = air temperature every month ($^{\circ}C$); $a = 6.75 \times 10^{-7} I^3 - 7.71 \times 10^{-5} I^2 - 1.79 \times 10^{-2} I - 0.492$; $I = (t_a/5)1.514$	3
$PE = \frac{\Gamma Q_n + \eta E_a}{\Gamma + \eta}$	Penman (1948)	Γ = slope of saturation vapor pressure; Q_n = net radiation (m/s); η = psychrometric constant (mmHg/ $^{\circ}C$); $E_a = (0.35 * 1 + 0.15 W_w)(p_{vsat}^{air} - p_v^a)$ (m/s); W_w = wind speed (km/h)	4
$PE = (0.457T + 8.13)p$	Blaney and Criddle (1950)	T = mean daily temperature ($^{\circ}C$); p = mean annual fraction of day which is in daylight	5
$PE = (0.025T + 0.078) \frac{R_s}{59}$	Jensen and Haise (1963)	R_s = incident solar radiation (mm/day)	6
$PE = \frac{1}{\lambda} \left[\frac{\Gamma A + \rho_a c_p D / r_a}{\Gamma + \eta(1 + r_s / r_a)} \right]$	Monteith (1965)	$A = R_n - G$ (MJ/m ² day); ρ_a = air vol heat capacity (MJ/m ³ $^{\circ}C$); D = portion in one day which is covered by sun; r_s, r_a = ratio between vapour transfer and canopy and aerodynamic resistance (day/m); c_p = the deficit in vapour pressure (kPa)	7
$PE = \alpha \frac{\Gamma}{\Gamma + \eta} (R_n - G)$	Priestley and Taylor (1972)	G = heat flux of soil (mm/day); α = empirical constant; R_n = radiation of sun (mm/day)	8
$PE = 0.0023 S_o \sqrt{S_T(T + 17.8)}$	Hargreaves et al. (1985)	S_T = the range of mean monthly minimum and maximum of temperature ($^{\circ}C$); S_o = radiation of sun (mm/day)	9

was utilized to evaluate the results from numerical analyses. Stability analyses were performed to evaluate the relationship between pore-water pressures and the slope's factor of safety. The extensive review on different method to calculate evaporation and the detailed development of procedure for analysing the actual evaporation are presented in this paper.

2 Theories of Evaporation

Researchers found that the actual evaporation (AE) from a surface of a soil corresponds to the soil relative humidity at the ground surface. The study by Sattler and Fredlund (1991) concluded that AE is approximately 70% of the potential evaporation (PE) in Saskatchewan, Canada. It is difficult to determine the relative humidity at the surface of the soil; however, it could be overcome if the overall suction and temperature of the soil at the ground surface are known. To date, there are two approaches developed by researchers to appraise the AE from uncovered soil bodies. The primary methodology depends on soil temperature and suction at the ground surface (Wilson et al. 1997; Blight 2009). The second depends on the actual vapor pressure and the ground surface's resistance (Tran et al. 2015). Different theories to calculate actual evaporation are summarized in Table 2.

The geo-environmental and geotechnical engineers started accepting soil suction more broadly when dealing with predictions of the rate of evaporation from ground surfaces. The results of the thin

soil area (with a thickness of 0.5–1 mm) analysis demonstrated that the actual evaporation is equivalent to the potential evaporation until soil suction surpasses the indicator around 3000 kPa of the total suction (Tran et al. 2015). Attempts have been made (Tran 2013) to find the soil suction where the AE from a ground surface starts to decrease from the PE. This is related to essential boundaries of an unsaturated soil (for example, the residual suction and the air-entry indicator) determined from SWCC.

The idea of "surface resistance" to the diffusion of vapor water was initiated by calculating the transpiration from the stomata of leaves and a tree shelter (Monteith and Szeicz 1961). In understanding and portraying the accurate evaporation resistance, the research works related to determination of surface resistance were growing rapidly. A method developed by Van de Griend and Owe (1994) estimates the resistance of the surface to the diffusion of vapor in drying soil at the soil near the ground surface. It was comprehended that surface resistance of fine sandy loam during the drying process began to increase at 15% soil volumetric water content within 0–1 cm depth. When soil cover water content and surface temperature are known, the soil cover moisture and surface resistance relationship can be expressed in an exponential form as the Penman equation for calculating the potential evaporation (PE). Equation 4 was suggested by Tran et al. (2015) to measure the Actual Evaporation using the moisture of the topsoil layer:

Table 2 Different theories to calculate actual evaporation

Equation	Theory	Definition of parameters	Equation No
$AE = \frac{\Gamma Q_a + \eta E_a}{\Gamma + \eta A}$	Modified Penman (Wilson 1990)	AE = actual evaporation; $E_a = 0.35(1 + 0.15W_w) p_v^d (B - A)$ (m/s); RH_{air} = relative humidity of air; $B = 1/RH_{air}$; RH = relative humidity; $A = 1/RH$	10
$AE = PE \left[\frac{RH - (p_{vsat}^{air}/p_{vsat})RH_{air}}{1 - (p_{vsat}^{air}/p_{vsat})RH_{air}} \right]$	Limiting function (Wilson et al. 1994)	p_{vsat} = saturated vapour pressure; p_{vsat}^{air} = vapour pressure at soil surface under saturated condition	11
$AE/PE = \exp\left(\frac{-\psi g \omega_v}{\zeta(1 - RH_{air})\gamma_w R(T + 273.15)}\right)$	Wilson et al. (1997)	R = universal gas constant; ω_v = molecular weight of water; ψ = total suction; T = soil temperature at the ground surface; $\zeta = 0.7$; g = acceleration of gravity; γ_w = unit weight of water	12

$$AE = \frac{Q_n + \frac{f'(u)}{f(u)} E_a}{+A \frac{f'(u)}{f(u)}} \tag{4}$$

$$\frac{f'(u)}{f(u)} = 1 + \frac{r_s}{r_{av}} \tag{5}$$

$$r_s = 10e^{0.3563(\theta_{min} - \theta_{top})} \tag{6}$$

where A is the inverse of the relative humidity of the soil, r_s =surface resistance at the top depth of 0–1 cm (s/m); r_{av} is the aerodynamic resistance to turbulent diffusion which is equal to 52 s/m; θ_{top} =volumetric water content in the 0–1 cm depth of top layer (in %); θ_R =volumetric water content corresponding to the reduction of the evaporation rate (in %). Originally van de Griend and Owe (1994) proposed that $\theta_R=15\%$ but a further study by Tran (2013) showed that θ_R is a function of soil properties and might be related to the SWCC curve of topsoil, hence θ_R could be calculated from the total suction associated with the reduction of evaporation rate.

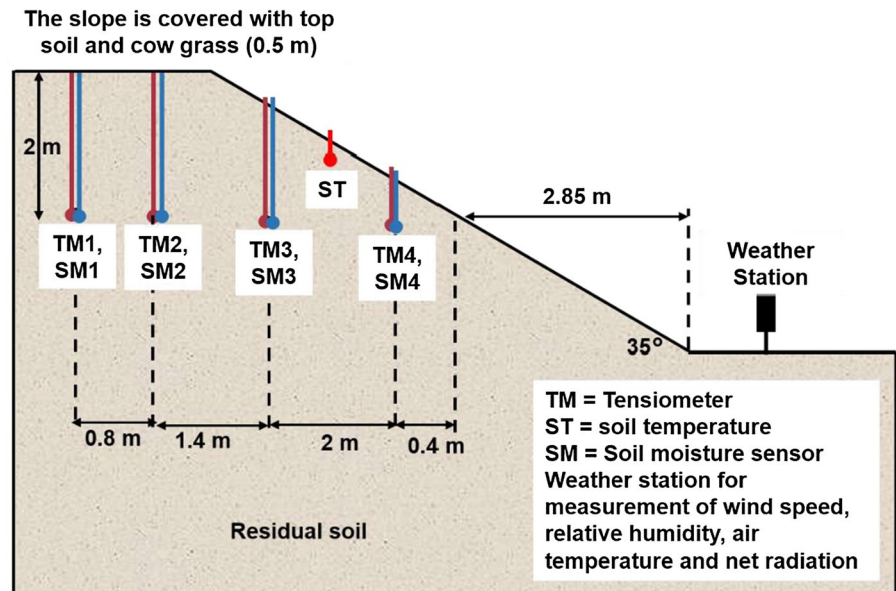
$$R = \begin{cases} a_{ev} \\ \frac{a_{res}}{a_{ev}} \times (1-a) \end{cases} \tag{7}$$

where ψ_{aev} =air-entry value (kPa); a =empirical factor varying between 0 and 1; θ_{res} =residual suction (kPa); Tran (2013) suggested to use $a=0.6$ for sand and 0.75 for silt.

3 Field Observation

A slope located at Orchard Boulevard in Singapore’s central areas was instrumented and monitored for six months period (1st July 2016–31st December 2016). The slope comprised of residual soil derived from Bukit Timah Granite with a height of 4 m and a slope angle of approximately 35°. Among the field measurements are climatic data (rainfall, air temperature, solar radiation, relative humidity, and wind speed), temperature and moisture of soil, and pore-water pressure distribution. The meteorological station for the measurements of the climatic parameters (Fig. 1) was situated near the toe of the slope. Soil temperature measurement was conducted at depths of 0.1 m, 0.15 m, 0.2 m, and 0.25 m. The slope was instrumented with soil moisture sensors and tensiometers which were installed at 2 m depth on the crest and at 0.4 m and 2.4 m of horizontal distances from slope face. Suction and soil moisture data at 0.4 m from slope face (a perpendicular distance of 0.23 m) were used as input to calculate actual evaporation in this study. There was no past record of slope failure in the

Fig. 1 Residual soil slope and instrumentation



region. Figure 1 shows the slope with the instrumentation locations.

Figure 2 shows the daily rainfall data at Orchard Boulevard from 1st July until 31st December 2016. The rainfall data collected from the slope during October were used in this study. The period was selected because there was a distribution of drying and wetting periods between 7 and 16th October. Besides, the highest intensity of rainfall and high rates of evaporation was observed within this period. This scenario was used to represent a cyclic period between drying and wetting in which evaporation was believed to have an important role. The wet period was identified on 7th, 9th, 13th, and 14th October, while the dry period was identified on 8th October, 10th to 12th October, and 15th to 16th October. The rainfall started at 6 am on 7th October and lasted for about 10 h with 20.8 mm/h of maximum intensity and 50.7 mm of total rainfall. There was no rain on 8th October. The rain started again at 6 am on 8th October and lasted only for one hour with an intensity of 16.3 mm. After about three days of no rain, which resulted in more significant negative pore-water pressures recorded by TM4, the slope was then exposed again to rainfall at 8 am on 13th October for an hour

with an intensity of 2.3 mm/hour. Lastly, the rain started again on 14th October with a total intensity of 54.2 mm/day which was the highest daily rainfall intensity used in this study.

The climatic data between July and December 2016 are presented in Table 3. It indicates that the highest air temperature was recorded in October 2016. The range of air temperature was between 25 and 35 °C. The maximum relative humidity of 99% was observed in November 2016. The range of relative humidity is between 64 and 99% from July to December 2016. The 2.5 m/s of maximum wind speed was observed in October 2016. The range of wind speed is between the lowest value of 0.84 m/s and the maximum value of 2.5 m/s from July to December 2016.

Figure 3 shows the plot of hourly rainfall from 7 to 16th October 2016. The cumulative rainfall during this period was 123.6 mm. The mean daily air temperature is shown in Fig. 4a, while the wind speed and relative humidity for this period are indicated in Fig. 4b. In addition, the climatic data, near-surface soil temperature, suction, and soil moisture were used to calculate actual evaporation following the Tran et al. (2015) method.

Fig. 2 Monthly and daily cumulative rainfall indicators from 1st July 2016 to 31st December 2016

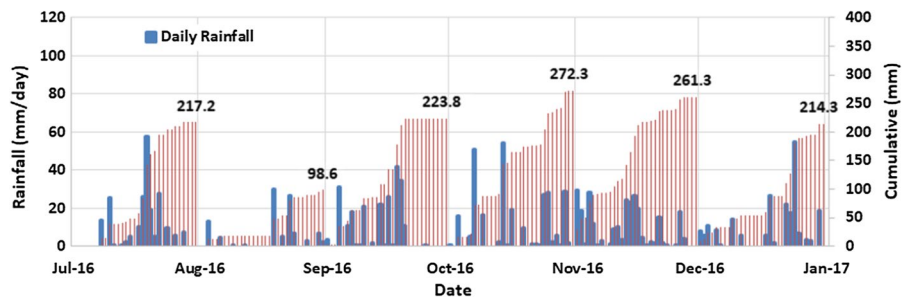


Table 3 Climatic data at Orchard between 1st July 2016 and 31st December 2016

	Jul	Aug	Sep	Oct	Nov	Dec
Total rainfall (mm)	217	98	22	272	311	214
Max Mean air temperature (°C)	32.5	32	31	35	30	31
Min Mean air temperature (°C)	26	25	26	27	25	29
Max Mean daily solar radiation (MJ/m ² /day)	12	14	12	12	12	12
Min Mean daily solar radiation (MJ/m ² /day)	2.0	4.0	1.0	1.5	1.1	1.7
Max Mean relative humidity (%)	96	90	92	97	99	91
Min Mean relative humidity (%)	74	70	64	69	73	66
Max daily wind speed (m/s)	1.22	1.30	2.08	2.50	1.58	4.51
Mean daily wind speed (m/s)	1.11	1.15	1.12	1.6	0.84	2.30

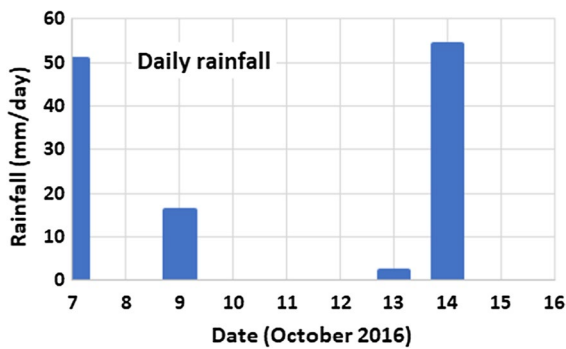


Fig. 3 Daily rainfall for the period from 7 to 16th October 2016

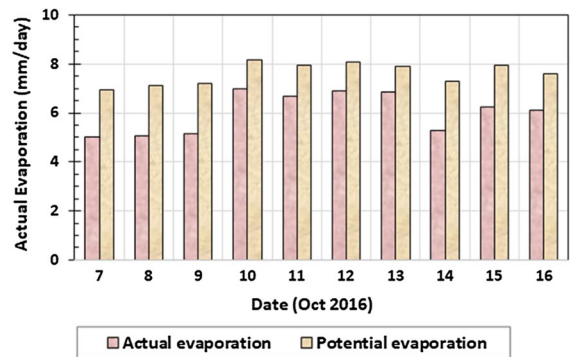


Fig. 5 Actual Evaporation calculated using Tran et al. (2015) equations for the period from 7 to 16th October 2016

The variation of soil temperature from 7 to 16th October is presented together with the variation of air temperature in Fig. 4a. The soil temperature was based on measurements at depth of 0.1 m since the soil temperature sensor was installed at this depth. The variations of potential and actual evaporations from 7 to 16th October are presented in Fig. 5. The maximum potential and actual evaporations were 8.2 mm/day and 7.1 mm/day, accordingly, as observed on 10th October 2016. The minimum potential and actual evaporations were 7 mm/day and 5 mm/day, correspondingly on 1st October 2016. As mentioned above, the calculation of actual evaporation using the Tran et al. (2015) equation required the establishment of the SWCC of surface

soil. The SWCCs of the topsoil (representing surface soil) and residual soil were obtained from the laboratory tests and the curves are indicated in Fig. 6. The air-entry value of the residual soil is 90 kPa whereas the air-entry value of the topsoil is 30 kPa. Measurements of the SWCC were carried out using Tempe cell (for suction values under 100 kPa) and Pressure plate (for suction values of 100–1500 kPa) (Rahardjo et al. 2019) by utilizing the axis translation technique as described in Satyanaga et al. (2019a). The drying curve of SWCC was used in this study since the results from Kristo et al. (2019) indicated that analyses using drying SWCC generated more conservative results. The best fitting procedure of the measured SWCC follow

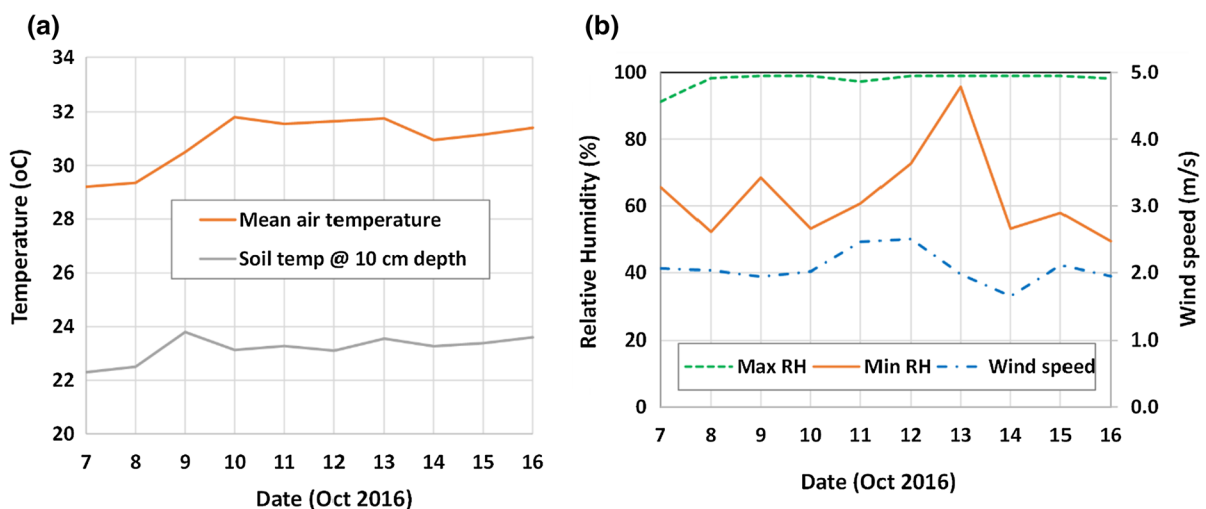


Fig. 4 Variation of **a** Air and Soil temperature **b** Wind speed and Relative humidity for the period from 7 to 16th October 2016

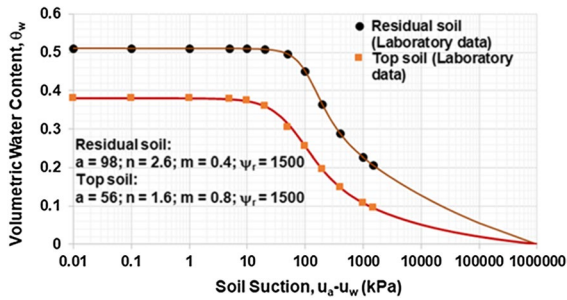


Fig. 6 SWCCs of residual soil and topsoil

the method explained in Satyanaga et al. (2017) and Zhai et al. (2020).

4 Numerical Model

The numerical model of seepage (SEEP/W) (Satyanaga and Rahardjo 2019a, b) was utilized to mimic the pore-water pressure variation obtained from the field measurements. Sections of flux were taken to find the rate of infiltration in the numerical model. In this study, two instances of transient seepage investigations were conducted. In Case 1 (the first instance), the rainfall was applied on the slope by assuming no evaporation was taking place during the dry weather days, while in Case 2 (the second instance), the actual evaporation together with rainfall infiltration was applied on the slope. Pore-water pressure measurements obtained from the instrumented slope were utilized to check the outcomes of the seepage analyses. The limit equilibrium slope stability analyses (SLOPE/W) (Satyanaga et al. 2019b) were used to calculate how the change in pore-water pressure impacted the safety factor of a slope. Bishop’s simplified model (Rahardjo et al. 2016a) was used to determine the factor of safety variation. The unsaturated shear strength properties were determined based on method proposed by Satyanaga and Rahardjo (2019b). The model of slope for slope stability and seepage analysis of the residual slope at Orchard Boulevard is shown in Fig. 7.

The SWCCs of topsoil and residual soil from the slope, as shown in Fig. 6, and the permeability function of the topsoil and residual soil from the slope as presented in Fig. 8 were utilized in the seepage analyses. The saturated permeability of the soil from

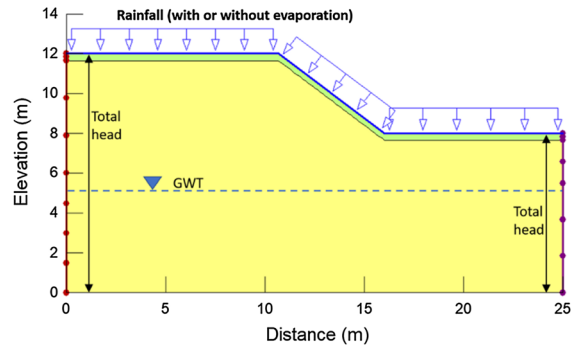


Fig. 7 Slope model for slope stability and seepage analysis

Orchard Boulevard as obtained from the laboratory experiment was 6×10^{-7} m/s, while the permeability functions of the analysed soils were computed from the SWCC curves utilizing the statistical model as explained by Rahardjo et al. (2016b).

The underlying condition for the slope model in Cases 1 and 2 was established by utilizing a spatial function (in the Seep/W program) for the first estimated pore-water pressures from the tensiometer recordings on 7th October 2016 when the rainfall started utilizing a spatial function (following procedures explained in Rahardjo and Satyanaga 2019a). The applied flux boundary conditions for Cases 1 and 2 are shown in Fig. 7. The distance between the edge of the slope model and the actual slope was specified to 3 times the slope height to prevent the effects of the side boundary conditions on the results of analysis. The soil layer from the ground surface down to a depth of 0.35 m was modelled as topsoil material. The finite element model in this region had a finer mesh size than those in other regions of the slope in

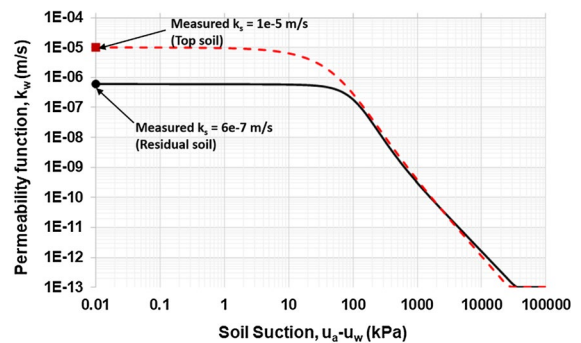


Fig. 8 Permeability function of topsoil and residual soil

order to acquire precise outcomes inside the infiltration area.

5 Results and Discussions

Figures 9 and 10 show the pore-water pressure variations measured by tensiometers between 7th October and 16th October 2016. The range of pore-water pressures between -20 and -50 kPa was observed around the soil surface on 11th October 2016. This might be attributed to the maximum evaporation of 8.1 mm/day that occurred on that day. The significant decrease in negative pore-water pressure occurred on 13th October 2016 from -50 into -25 kPa within the depth of 2.5 m from the surface of the slope. This happened due to the heavy rainfall of 54.2 mm/day. The field monitoring results were correlated with the results from the numerical analyses of Case 1 and Case 2. It was observed that the profiles of pore-water pressure from the numerical analyses of Case 2 were closer to the field monitoring results in comparison with those from the numerical analyses of Case 1. The comparison shows the importance of incorporating the actual evaporation in numerical experiments.

The variations in factors of safety from the numerical analyses of Cases 1 and 2 are indicated in Fig. 11. These are generated according to the incorporation of negative pore-water pressures from the seepage analyses of both cases. It can be noticed that the overall factors of safety for Case 1 were much lower as compared to those for Case 2 at all the times. The significant differences in the factor of safety between Case 1 and Case 2 were observed on $t=7$ days (13th October 2016). The minimum factor of safety on 13th October 2016 for Case 1 was 1.15 , whereas the minimum

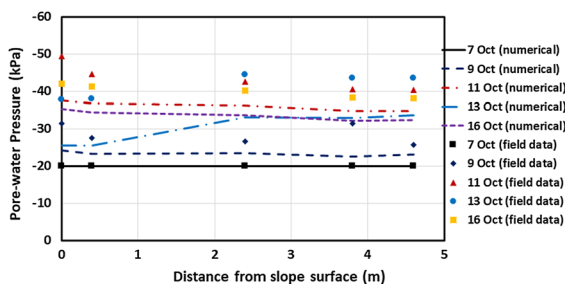


Fig. 9 Pore-water pressure variations from field data and numerical analyses without actual evaporation

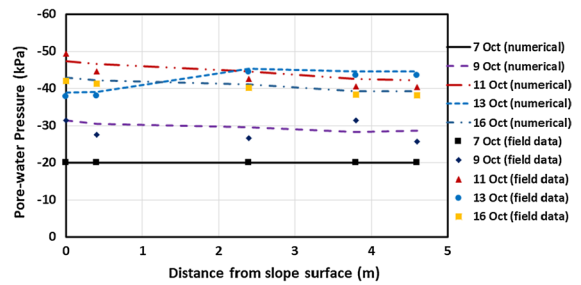


Fig. 10 Pore-water pressure variations from field data and numerical analyses with actual evaporation

factor of safety on 13th October 2016 for Case 2 was 1.35 . These differences were attributed to the high evaporation rate at the Orchard slope before 13th October 2016.

Figure 11 demonstrates the importance of incorporating the actual evaporation in calculating the factor of safety for residual soil slopes. The exclusion of the actual evaporation in the stability analyses may lead to unnecessary rectification measures for the slope. The other factors which may influence the pore-water pressure distributions and factor of safety variations obtained from the numerical analyses are the variability of SWCC from laboratory testing. Zhai and Rahardjo (2013) concluded that the SWCC from the experimental works using the same equipment, specimen size, testing duration and same method of testing may vary. They suggested to carry out experimental works of SWCC based on the maximum matric suction and the minimum number of data points to obtain an acceptable SWCC. The experimental works in this study were conducted following the required

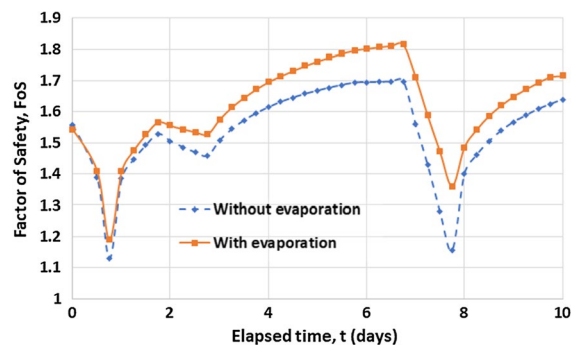


Fig. 11 Variations in the factor of safety based on numerical analyses with and without evaporation

maximum suction and minimum number of data points as suggested by Zhai and Rahardjo (2013) to generate reasonable results of SWCC. Different methods in the determination of actual evaporation may also affect the results of seepage and stability analyses. Review of different theories on the determination of actual evaporation has been conducted in this study. Tran et al (2015) method was considered the best method to estimate the actual evaporation. Therefore, the pore-water pressures and factor of safety variations from this study are considered reasonable. In addition, the results from the numerical analyses were in agreement with the results from the field instrumentation.

6 Conclusions

The results of this research can be summarised as follows:

1. Tran et al. (2015) technique can be utilized to quantify the actual evaporation since the calculated results were reasonable as compared to the potential evaporation (PE) based on the Penman method.
2. The numerical analyses incorporating the actual evaporation generate more representative pore-water pressures variations as compared to the analyses ignoring the actual evaporation
3. A realistic variation of the factor of safety of a residual soil slope can be obtained by incorporating the actual evaporation and rainfall in the slope stability and seepage analyses.

Acknowledgements This research was supported by the Nazarbayev University Research Fund under Social Policy Grant and 11022021CRP1512. Any opinions, findings, and conclusions or recommendations expressed in this material are those of the author(s) and do not necessarily reflect the views of the Nazarbayev University.

Funding Funding is provided by Nazarbayev University (Grant No. 11022021CRP1512 and Social Policy Grant).

Data Availability Enquiries about data availability should be directed to the authors.

Conflict of interest The authors have not disclosed any conflict of interest.

References

- Blaney HF, Criddle WD (1950) Determining water requirements in irrigated area from climatological irrigation data. US Dep. of Agr. Tech. Pap. No. 96. 48 p.
- Blight G (2009) Solar heating of the soil and evaporation from a soil surface. *Géotechnique* 59(4):355–363
- Fredlund DG, Rahardjo H (1993) Soil mechanics for unsaturated soils. Wiley
- Fredlund DG, Rahardjo H, Fredlund MD (2012) Unsaturated soil mechanics in engineering practice. Wiley
- Gitirana Jr. G, Fredlund DG, Fredlund M (2006) Numerical modeling of soil-atmosphere interaction for unsaturated surfaces. In: Proceedings of the 4th international conference on unsaturated soils, Arizona, 2–6 April 1, pp 658–669
- Hargreaves GL, Hargreaves GH, Riley JP (1985) Irrigation water requirements for Senegal river basin. *J Irrig Drain Eng* 111:265–275
- Ip CY, Rahardjo H, Satyanaga A (2021) Three-dimensional slope stability analysis incorporating unsaturated soil properties in Singapore. *Georisk Assess Manag Risk Eng Syst Geohazards* 15(2):98–112
- Jensen ME, Haise HR (1963) Estimating evapotranspiration from solar radiation. *J Irrig Drain Div* 89:15–41
- Kristo K, Rahardjo H, Satyanaga A (2019) Effect of hysteresis on the stability of residual soil slope. *Int Soil Water Conserv Res* 7(3):226–238
- Li AG, Yue Tham LG, Lee CF (2005) Field-monitored variations of soil moisture and matric suction in a saprolite slope. *Can Geotech J* 42:13–26
- Monteith JL (1965) Evaporation and environment. *Symp Soc Exp Biol* 19:205–234
- Monteith JL, Szeicz G (1961) The radiation balance of bare soil and vegetation. *J Roy Meteorol Soc* 87(372):159–170
- Newson TA, Fahey M (2003) Measurement of evaporation from saline tailings storages. *Eng Geol* 70(3):217–233
- Ng CWW, Springman SM, Alonso EE (2008) Monitoring the performance of unsaturated soil slopes. *Geotech Geol Eng* 26(6):799–816
- Pierre G, Régis M, Madjid D, Frédéric D (2019) Influence of climatic conditions on evaporation in soil samples. *Environ Geotech* 6(6):323–333
- Priestley CHB, Taylor RJ (1972) On the assessment of surface heat flux and evaporation using large scale parameters. *Mon Weather Rev* 100:81–92
- Rahardjo H, Satyanaga A (2019) Sensing and monitoring for assessment of rainfall-induced slope failures in residual soil. *Geotech Eng* 172(6):496–506
- Rahardjo H, Satyanaga A, Leong EC, Wang JY (2014) Comprehensive instrumentation for real time monitoring of flux boundary conditions in slope. *Proc Earth Planet Sci* 9:23–43
- Rahardjo H, Satyanaga A, Harnas FR, Leong EC (2016) Use of dual capillary barrier as cover system for a sanitary landfill in Singapore. *Indian Geotech J* 46(3):228–238
- Rahardjo H, Satyanaga A, Mohamed H, Ip CY, Rishi SS (2019) Comparison of soil–water characteristic curves from conventional testing and combination of small-scale

- centrifuge and dew point methods. *J Geotech Geol Eng* 37(2):659–672
- Rahardjo H, Satyanaga A, Leong EC (2016b) Effects of rainfall characteristics on the stability of tropical residual soil slope. In: Proceedings of E-UNSAT 2016, E3S web of conferences 9, Sep 2016, vol 15004, pp 1–6
- Raj AS, Oliver DH, Srinivas Y, Viswanath J (2017) Wavelet based analysis on rainfall and water table depth forecasting using neural networks in Kanyakumari district, Tamil Nadu, India. *Groundwater Sustain Dev* 5:178–186
- Rohwer C (1931) "Evaporation from free water surfaces," Technical Bulletins 163103, United States Department of Agriculture, Economic Research Service
- Sattler PJ, Fredlund DG (1991) Modeling vertical ground movements using surface climatic flux. In: Proceedings of geotechnical engineering congress, Boulder Colorado, June 10–12, vol 2, pp 1292–1306
- Satyanaga A, Rahardjo H (2019a) Stability of unsaturated soil slopes covered with *Melastoma malabathricum* in Singapore. *Proc Inst Civil Eng Geotech Eng* 172(6):530–540
- Satyanaga A, Rahardjo H (2019b) Unsaturated shear strength of soil with bimodal soil-water characteristic curve. *Geotechnique* 69(9):828–832
- Satyanaga A, Rahardjo H (2020) Role of unsaturated soil properties in the development of slope susceptibility map. *Geotech Eng*. <https://doi.org/10.1680/jgeen.20.00085>
- Satyanaga A, Zhai Q, Rahardjo H (2017) Estimation of unimodal water characteristic curve for gap-graded soil. *Soils Found* 57(5):789–801
- Satyanaga A, Rahardjo H, Koh ZH, Mohamed H (2019a) Measurement of a soil-water characteristic curve and unsaturated permeability using the evaporation method and the chilled-mirror method. *J Zhejiang Univ Sci A* 20(5):368–375
- Satyanaga A, Rahardjo H, Hua C (2019b) Numerical simulation of capillary barrier system under rainfall infiltration in Singapore. *Int J Geoenviron Eng* 5(1):43–54
- Thornthwaite CW, Holzman B (1942) Measurement of evapotranspiration from land and water surfaces. USDA Technical Report. No. 817
- Thornthwaite CW (1948) An approach toward a rational classification of climate. *Geogr Rev* 38(1):55–94
- Tran DTQ, Fredlund DG, Chan DH (2015) Improvements to the calculation of actual evaporation from bare soil surfaces. *Can Geotech J* 53:118–133
- Tran DTQ (2013) Re-visitation of actual evaporation theories. Ph.D. thesis, University of Alberta, Edmonton, Alta
- Van de Griend AA, Owe M (1994) Bare soil surface resistance to evaporation by vapor diffusion under semiarid conditions. *Water Resour Res* 30(2):181–188
- Wilson GW, Fredlund DG, Barbour SL (1994) Coupled soil-atmosphere modeling for soil evaporation. *Can Geotech J* 31(2):151–161
- Wilson GW, Fredlund DG, Barbour SL (1997) The effect of soil suction on evaporative fluxes from soil surfaces. *Can Geotech J* 34:145–155
- Wilson GW (1990) Soil evaporative fluxes for geotechnical engineering problems. Ph.D. Thesis, University of Saskatchewan, Saskatoon, SK., Canada
- Zhai Q, Rahardjo H (2013) Quantification of uncertainties in soil-water characteristic curve associated with fitting parameters. *J Eng Geol* 163:144–152
- Zhai Q, Rahardjo H, Satyanaga A (2019) Estimation of the air permeability function from the soil-water characteristic curve. *Can Geotech J* 56(4):505–513
- Zhai Q, Rahardjo H, Satyanaga A, Dai G (2019) Role of the pore-size distribution function on water flow in unsaturated soil. *J Zhejiang Univ Sci A* 20(1):10–20
- Zhai Q, Rahardjo H, Satyanaga A, Dai G, Zhuang Y (2020) Framework to estimate the soil-water characteristic curve for soils with different void ratios. *Bull Eng Geol Env* 79(8):4399–4409

Publisher's Note Springer Nature remains neutral with regard to jurisdictional claims in published maps and institutional affiliations.